Applying U-Pb chronometry and trace element geochemistry of apatite to carbonatite-phoscorite complexes – as exemplified by the 2.06 Ga Phalaborwa Complex, South Africa

L.Y. Le Bras

School of Geosciences, University of the Witwatersrand, Braamfontein, 2001, Johannesburg, South Africa
e-mail: loic.y.lebras@gmail.com

L. Milani

Department of Geology, University of Pretoria, Private Bag X20, Hatfield 0028, South Africa
e-mail: lorenzo.milani@up.ac.za

R. Bolhar

School of Geosciences, University of the Witwatersrand, Braamfontein, 2001, Johannesburg, South Africa
e-mail: robert.bolhar@wits.ac.za

G. O'Sullivan

UCD School of Earth Sciences, University College Dublin, Belfield, Dublin 4, Ireland
e-mail: gjosulli@tcd.ie

Abstract

Uranium-lead dating of apatite was undertaken by Laser Ablation-Sector Field-Inductively Coupled Plasma Mass Spectrometry (LA-SF-ICPMS) *in situ* on apatite from principal rock types of the Loolekop phoscorite-carbonatite intrusion within the Phalaborwa Igneous Complex, South Africa. *In situ* U-Pb analysis on selected apatite produces U-Pb ages of 2 083.9 ± 41.9 Ma (n = 33; MSWD = 0.87), 2 020.4 ± 116.7 Ma (n = 18; MSWD = 0.91) and 2 034.3 ± 39.0 Ma (n = 17; MSWD = 0.6) for phoscorite, banded carbonatite and transgressive carbonatite, respectively, with a combined age of 2 054.3 ± 21.4 Ma (n = 68; MSWD = 0.86), which we interpret to indicate the timing of emplacement. Apatite U-Pb dates are similar to dates reported in previous studies using zircon and baddeleyite U-Pb systems from the same rock types, showing that apatite can be used as geochronometer in the absence of other commonly used U-Pb-bearing accessory minerals, not only in carbonatite-phoscorite complexes, but in all mafic igneous intrusions. Similar ages for zircon, baddeleyite and apatite indicate little to no re-equilibration of the latter, and suggest that the Loolekop Pipe intrusion cooled below 350°C within ~21 Ma of emplacement. This conclusion is supported by apatite BSE images and trace element systematics, with unimodal igneous trace element characteristics for apatite in each sample. The combination of *in situ* U-Pb geochronology, trace element geochemistry and BSE imaging makes apatite a useful tool to investigate the emplacement mechanisms of carbonatite-phoscorite complexes, which is particularly advantageous as apatite is one of the main mineral phases in these rock suites.

Introduction

The Loolekop phoscorite-carbonatite sequence of the Phalaborwa Igneous Complex has been extensively studied over the past few decades, including Cu mineralisation (Forster, 1958; Heinrich, 1970; Bulakh et al., 1998; Du Plessis, 2019; Le Bras, 2021a, b), the composition of silicate, phosphate, carbonate, oxide and Rare Earth Elements (REE)-bearing minerals (Dawson and Hinton, 2003; Giebel et al., 2017, 2019; Milani et al., 2017a, b) and Pb-S isotopes in sulphides (Bolhar et al., 2020). Uranium-lead zircon and baddeleyite geochronology (Eriksson, 1984; Heaman and LeCheminant, 1993; Wu et al., 2011) has allowed to establish the relative timing of emplacement of the different rock types, specifically the sequence comprising phoscorite-calcite carbonatite (hereafter termed banded carbonatite), as well as the late-stage Mg-rich calcite carbonatite (hereafter referred to as transgressive carbonatite).

The U-Pb system in apatite has emerged as a medium-temperature geo- and thermo-chronometer (Chew et al., 2011; Chen and Simonetti, 2013; Cochrane et al., 2014; Chew and Spikings, 2015; O'Sullivan et al., 2020, 2021). Apatite is common in igneous, metamorphic and sedimentary rock types with wide-ranging chemical compositions (Piccoli and Candela, 2002). The combined use of U-Pb geochronology, trace element geochemistry, scanning electron microscopy (SEM) to collect backscattered electron (BSE) images, and semi-quantitative analyses via energy dispersive X-ray (EDX) spectroscopy, renders apatite a powerful tool for understanding processes like metasomatism, metamorphism, and the reconstruction of the thermal histories of igneous and sedimentary systems (Harlov, 2015; Kirkland et al., 2017, 2018; Henrichs et al., 2018; O'Sullivan et al., 2021). In phoscorite-carbonatite intrusions, apatite is one of the major rock-forming minerals, together with magnetite, carbonates and Mg-rich silicates (e.g. diopside, phlogopite, forsterite) (Krasnova et al., 2004; Milani et al., 2017a, b). In this paper, we test the potential of the apatite geochronometer to infer the crystallisation and cooling history of phoscorite-carbonatite magmatic systems, where apatite is abundant and can easily be analysed *in situ*. The use of U-Pb apatite geochronology may not provide the required precision for these purposes (as apatite in mafic igneous systems typically has lower concentrations of U compared to apatite in felsic systems, O'Sullivan et al., 2020). However, the combination of U-Pb ages with geochemistry in apatite can represent a novel approach to a better understanding of emplacement and cooling histories of this type of igneous complex as well as a useful tool in the absence of other conventional geochronometers.

Geological setting
The Phalaborwa Igneous Complex

The Phalaborwa Igneous Complex is located in the Limpopo Province, South Africa (Figure 1), and results from the emplacement of several successive magma pulses into granites and gneisses of the Kaapvaal Craton, forming an 18.5 km^2 kidney-shaped intrusion (Heinrich, 1970; Eriksson, 1982). The complex is composed of three feeding pipes forming three adjacent North-South aligned lobes (Eriksson, 1982, 1989). The Phalaborwa Igneous Complex is dominated by a unit of pyroxenite with variable proportions of phlogopite, diopside and apatite, which interacted during the emplacement with the gneisses and granites of the Kaapvaal Craton to form an aureole of feldspathic pyroxenite at the contact with the basement rocks (Lombaard et al., 1964; Hanekom et al., 1965; Eriksson, 1982; Giebel et al., 2019). Phlogopite is locally altered to vermiculite through surficial weathering (Fourie and de Jager, 1986). Subsequently, pyroxene-bearing pegmatites of various compositions crystallised in each of the intrusive centres. Later, dolerite dikes intruded throughout the region, striking northeast-southwest.

The Loolekop Pipe

The Loolekop Pipe is located in the centre of the Phalaborwa Igneous Complex and formed from three near-synchronous magma pulses that intruded the micaceous pyroxenite. Phoscorite forms the marginal part of the pipe, at the contact with the pyroxene pegmatite, while banded carbonatite was emplaced towards the core of the pipe (Palabora Mining Company, 1976; Eriksson, 1982). Subvertical mineral alignments form a progressive transition from phoscorite at the margins of the pipe, to banded carbonite at the centre of the pipe (Figure 1). Phoscorite comprises olivine (often serpentinised or replaced by chondrodite), diopside, magnetite, apatite, phlogopite and minor calcite (Lombaard et al., 1964; Hanekom et al., 1965; Heinrich et al., 1970). Banded carbonatite consists of calcite with dolomite, apatite, magnetite and minor phlogopite, monazite, rare olivine (Palabora Mining Company, 1976; Eriksson, 1989) and is characterised by a distinct banded texture defined by alignment of apatite, magnetite and phlogopite.

The emplacement of the phoscorite-carbonatite sequence was followed by a structural event causing a fracturing of the pipe and producing a resurgence of igneous activity (Heinrich, 1970). The latest triggered the subsequent ascent of a second carbonatitic pulse and emplacement of the transgressive carbonatite (composed of calcite and dolomite, with minor magnetite and apatite). The Loolekop Pipe represents the world's only known carbonatite-phoscorite-hosted Cu-sulphide deposit of economic interest. Recently, a sulphide Pb-Pb age of 2 054 ± 99 Ma was obtained using SIMS to constrain the timing of mineralisation within all three principal rock types (Bolhar et al., 2020).

Palaeoproterozoic ^{207}Pb/^{206}Pb weighted ages for phoscorite (2 047 ± 27 Ma, n = 6, MSWD = 0.4 for zircon; 2 061.7 ± 2.4 Ma, n = 30, MSWD = 1.5 for baddeleyite), banded carbonatite (2 060.0 ± 2.2 Ma, n = 30, MSWD = 1.8 for baddeleyite) and transgressive carbonatite (2 053 ± 14 Ma, n = 14, MSWD = 1.5 for zircon; 2 059.8 ± 1.3 Ma, n = 30, MSWD = 0.8 and 2 056.7 ± 2.7 Ma, n = 30, MSWD = 1.2 for baddeleyite) have been used to suggest a quasi-coeval emplacement of the intrusive bodies (Wu et al., 2011).
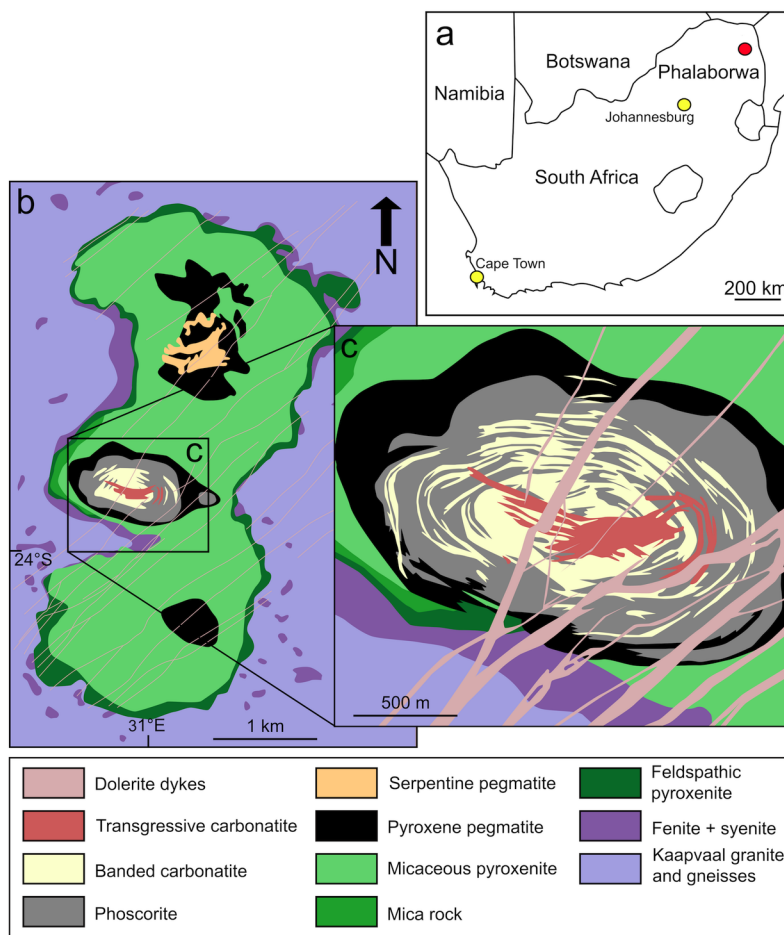
Figure 1. (**a**) *Regional map indicating the location of the Phalaborwa Igneous Complex.* (**b**) *Simplified geological map of the Phalaborwa Igneous Complex.* (**c**) *Enlarged view on the Loolekop carbonatite – phoscorite intrusion (modified from Basson et al., 2017 and references therein).*

Sample material and methods
Samples

Several representative samples were collected at the Palabora Mining Company drill core yard: Three samples of phoscorite (B60Ph, B61Ph and GC813CPh), two samples of banded carbonatite (GC813ABC and JKCBC) and two samples of transgressive carbonatite (B63A and JKTC). One section was made per sample. Only orthomagmatic primary apatite has been analysed, avoiding secondary apatite, related to late-stage interaction with H_2O-C-rich fluids (ap-II and ap-III, Giebel et al., 2019).

Laser Ablation SF-ICP-MS

Analysis of U-Pb isotope ratios (75 spots) were performed in the Earth Lab at the University of the Witwatersrand, Johannesburg, South Africa, using a Thermo Fisher Scientific Element XR SF-ICPMS coupled to a 193 nm excimer Applied Spectra/Australian Scientific Instruments RESOlution-SE laser ablation system. The sample surface was pre-ablated using two laser pulses to remove surface Pb before each spot measurement. All measurements were made using a laser spot diameter of 64 µm, a repetition rate of 10 Hz and a laser fluence of 3.00 J cm^{-2}. Background was measured for 5 seconds before and after ablation and the sample measurement lasted for 20 seconds. The Madagascar apatite was used as primary calibration standard (Thomson et al., 2012). Secondary reference materials included McClure Mountain (Schoene and Bowring, 2006) and Durango (McDowell et al., 2005) apatite. [207]Pb corrected ages (using the method of Chew et al., 2011) were 543 +/- 24 Ma (MSWD = 3.7, n = 6) and 31.9 +/- 1.2 Ma (MSWD = 1.3, n = 10) for McClure and Durango apatite, respectively. Data were processed using the software Iolite v3.7 (Paton et al., 2011) and the ages were calculated using IsoplotR (Vermeesch, 2018).

Apatite trace elements (98 spots) were measured by LA-ICPMS at the Central Analytical Facility (CAF) of Stellenbosch University, South Africa. The experimental set-up consisted of an excimer laser ablation system (Resonetics Resolution S155-LR utilising a Coherent CompexPro 110 laser source emitting at 193 nm), coupled to an Agilent 7700ce quadrupole ICP-MS. Analytical details, including accuracy and precision, analytical results and a preliminary discussion of the data are reported in Milani et al. (2017b).

Results

Apatite appearance

Apatite is present in all lithologies of the complex and occurs in a variety of shapes, sizes, and textures, from anhedral to euhedral prismatic, from mm- to cm-size, concurring to define the layering in the banded carbonatite (Figure 2a to f e.g. Milani et al., 2017b). Apatite tends to be aggregated in subhedral shapes interstitial to olivines in the phoscorite (Figure 2a to c). Optical microscopy does not reveal distinct patterns or zonations, but BSE images show in large apatite crystals weak concentric zoning parallel to their boundaries (Figure 3a to e) as well as patchy zoning

(Figure 3c to f). Smaller apatite crystals may occur as inclusions in olivine and phlogopite, while monazite rims can be observed, interpreted as the result of dissolution/reprecipitation processes during REE-rich hydrothermal fluid interaction (e.g. Putnis, 2009; Harlov, 2015; Giebel et al., 2017). Occasional formation of secondary apatite has been observed at late magmatic and even at post-sulphide stages (e.g. Giebel et al., 2017).

U-Pb geochronology

The U-Pb isotopic data collected by LA-SF-ICPMS analysis is reported in Table 1. Apatite from all three principal rock types
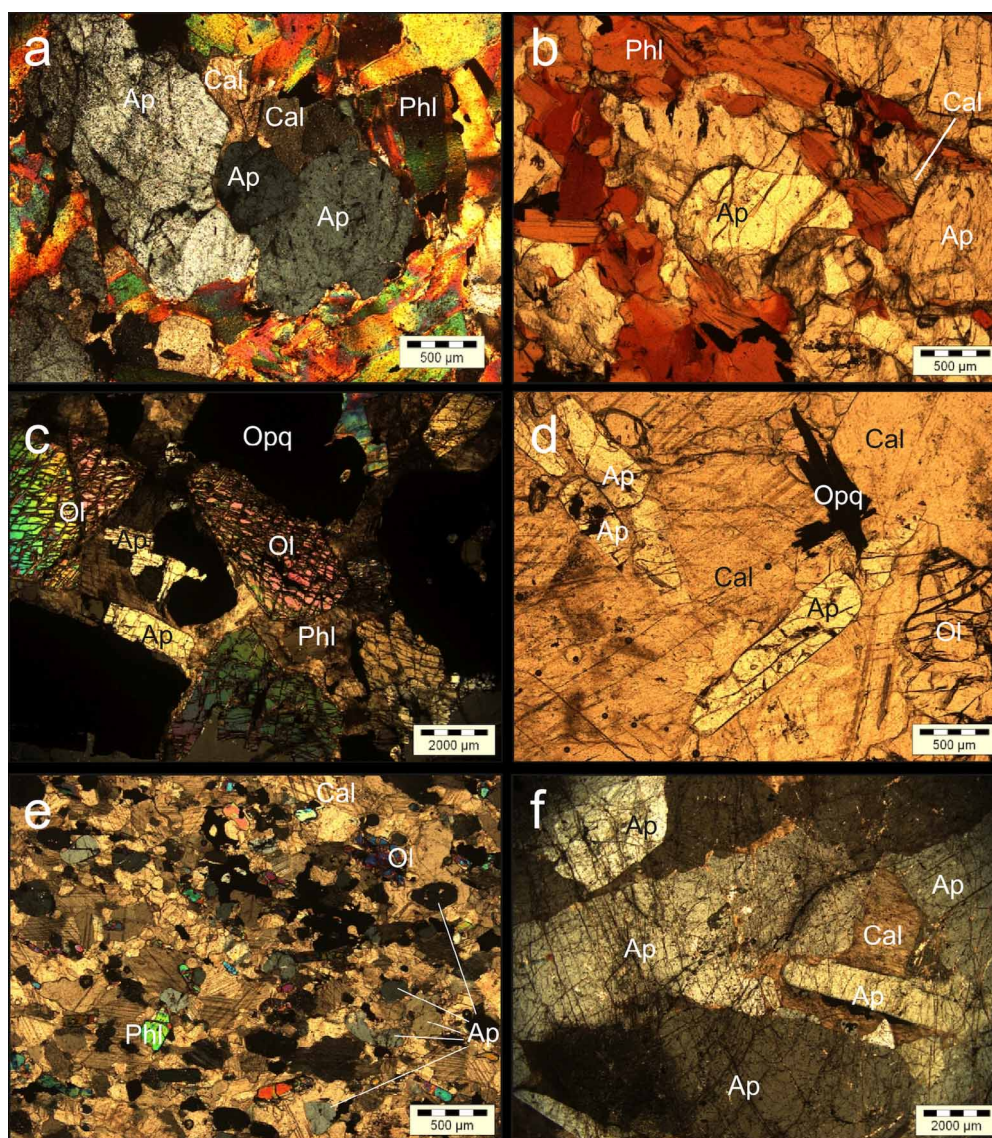
Figure 2. *Representative photomicrographs of the studied samples, in transmitted light. (a) Large subhedral apatite crystals and rare calcite as aggregates in phlogopite in phoscorite B60 (cross polarised light, XPL). (b) Elongated and partially iso-oriented phlogopite and large anhedral apatite in phoscorite B61 (plane polarised light, PPL). (c) Cumulitic magnetite (as Opq) and cm-scale olivine in phoscorite GC813C with minor apatite interstitial to, or embedded in, magnetite (XPL). (d) Clusters of elongated euhedral apatite in calcite, with minor opaques and subhedral olivine in banded carbonatite GC813A (PPL). (e) Subhedral rounded apatite crystals punctuate banded carbonatite JKCBC, with phlogopite and magnetite defining a weak rock banding (PPL). (f) Patches of large apatite as prismatic, sub-rounded and stubby crystals in transgressive carbonatite BC63A (XPL). Abbreviations: Ap=apatite; Cal=calcite; Ol=olivine; Opq=opaques; Phl=phlogopite.*
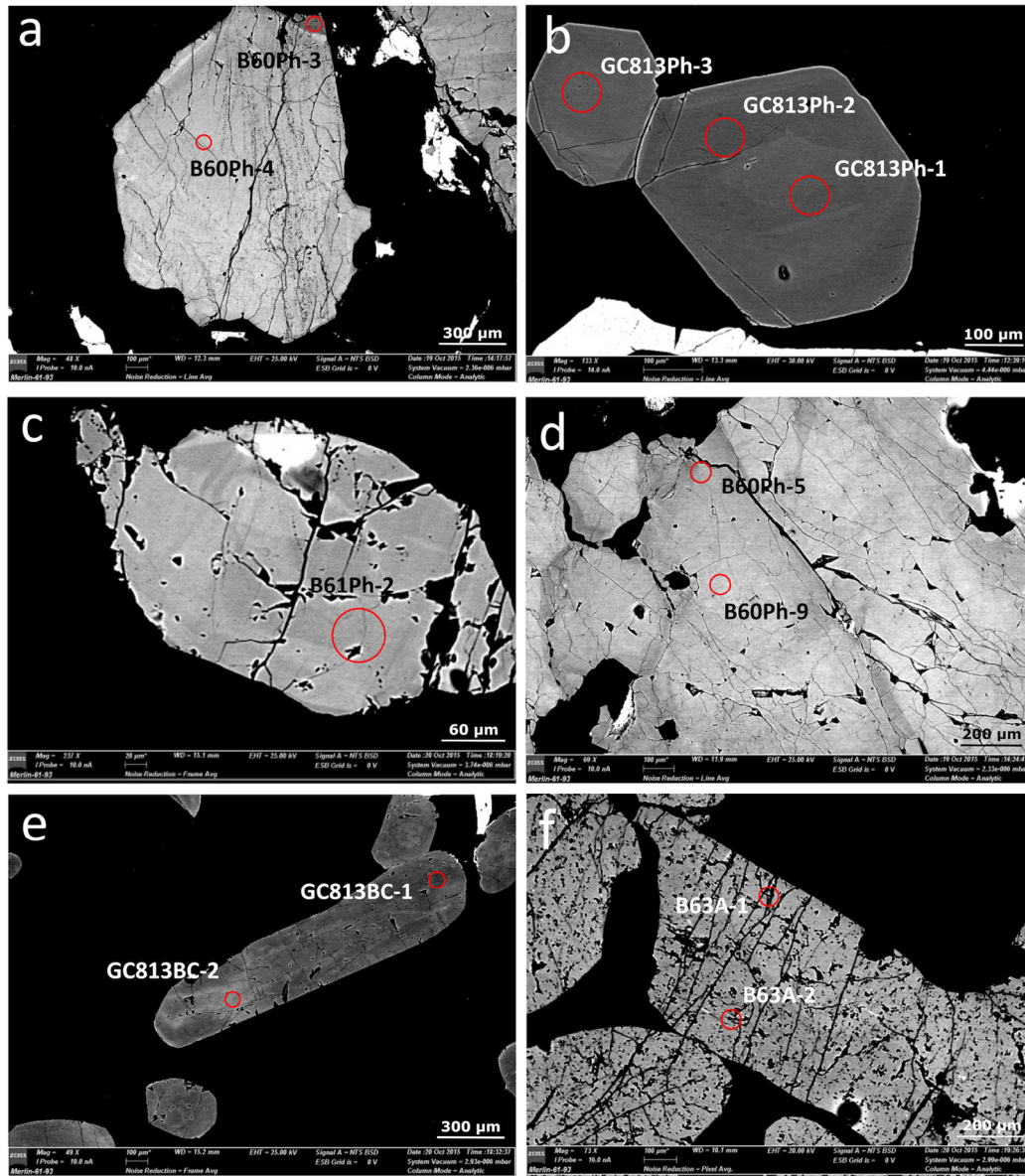
Figure 3. *Back scattered images of apatite grains in (**a**),(**b**),(**c**) and (**d**) phoscorite, (**e**) banded carbonatite and (**f**) transgressive carbonatite with locations of LA-ICP-MS analysis spots.*

yield identical ages within analytical uncertainty (2 SE). Phoscorite-hosted apatite produces a Tera-Wasserburg discordia lower-intercept date of 2 083.9 ± 41.9 Ma (n = 33; MSWD = 0.87) (Figure 4a), banded carbonatite-hosted apatite yields a lower-intercept age of 2 020.4 ± 116.7 Ma (n = 18; MSWD = 0.91) (Figure 4b), and transgressive carbonatite-hosted apatite produces a lower-intercept age of 2 034.3 ± 39.0 Ma (n = 17; MSWD = 0.6) (Figure 4c). All ages were regressed without anchoring to an assumed common Pb isotopic composition. Combining apatite from all lithologies gives a Tera-Wasserburg discordia lower-intercept date of 2 054.3 ± 21.4 Ma (n = 68; MSWD = 0.86) (Figure 4d). The common Pb upper intercepts for apatite discordia from phoscorite, banded and transgressive carbonatite are 0.94 ± 0.18, 0.85 ± 0.26 and 0.87 ± 0.05, respectively.

Ages were also calculated using an anchored $^{207}Pb/^{206}Pb$ ratio acquired from the composition of the least radiogenic sulphides in the complex (0.97, Bolhar et al., 2020), translating into apparent Tera-Wasserburg discordia lower-intercept dates of 2 108.5 ± 24.3 Ma, 2 128.6 ± 61.2 Ma and 2 110.89 ± 35.6 Ma for phoscorite, banded- and transgressive carbonatite, respectively. These dates are consistently older than the unanchored ones and indicate that the $^{207}Pb/^{206}Pb$ ratio in apatite is higher when compared to sulphides in the Loolekop Pipe.

Assessment of apatite chemical data from the literature

Microprobe analyses demonstrate that apatite at Phalaborwa is typically fluorapatite with low or negligible chlorine (Milani et al., 2017b; Giebel et al., 2019; Decrée et al., 2020). The trace
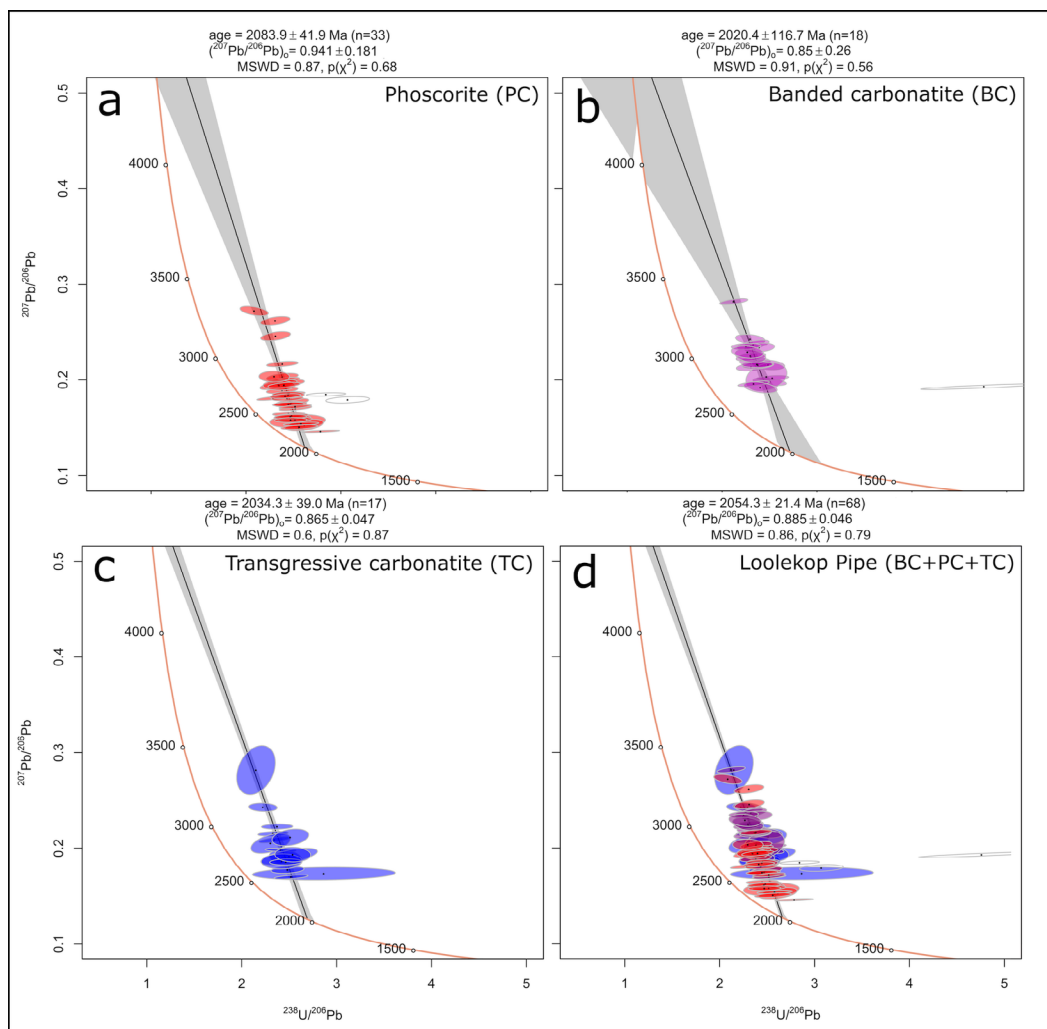
Figure 4. *Tera-Wasserburg diagrams and lower intercept ages for (**a**) phoscorite, (**b**) banded carbonatite, (**c**) transgressive carbonatite and (**d**) combined from the three rock types. Graphs were generated using IsoplotR, (Vermeesch, 2018).*

element composition of apatite has previously been studied in conjunction with calcite and other mineral phases to infer a common mantle source for the phoscorite-carbonatite association (Milani et al., 2017b). Trace elements in apatite can aid interpretation of U-Pb ages and constrain crystallisation dynamics and magma fractionation processes, especially when combined with BSE imaging. Relevant element and chondrite-normalised element ratios contents are reported in Table 2, while the full dataset of analysed apatite can be retrieved from the Supplementary Material. (A supplemetary data file is archived in the South African Journal of Geology repository (https://doi.org/10.25131/sajg.125.0015.sup-mat)).

Trace elements in apatite from all of the analysed rock types in Phalaborwa are uniform within each sample, with only slight differences between spots (Figure 5a). Three transgressive carbonatite-hosted apatites (out of 18) show depletion in U and Th relative to other apatite in the same rock. In phoscorite, chondrite-normalised Th and U concentrations vary by one order of magnitude, whilst in the banded and transgressive carbonatite, intra-sample variation is more limited (varying only by a factor of

two). The Eu/Eu* ratios of apatite are mostly in the range of apatite from worldwide carbonatites (= 0.85 to 1.16, e.g. Mao et al., 2016), as in phoscorite, banded and transgressive carbonatite averages are of 0.86, 0.83 and 0.85, and range from 0.80 to 1.10 (n = 51), 0.67 to 0.90 (n = 31) and 0.83 to 0.88 (n = 18), respectively. Chondrite-normalised REE patterns show enrichment in LREE relative to HREE (Figure 5b). $(La/Sm)_{ch}$ ratios show a wider variation interval in phoscorite (1.72 to 10.2) relative to banded and transgressive carbonatite (1.34 to 2.88 and 2.02 to 2.84, respectively; Table 2). $(La/Yb)_{ch}$ ratios also vary significantly in phoscorite (70.7 to 334) when compared with banded carbonatite (114 to 213) and transgressive carbonatite (116 to 238). The total amount of REE in apatite shows a significant variation in both phoscorite (5 908 to 51 498 ppm, median of 12 357) and banded carbonatite (8 381 ppm to 20 897 ppm, median of 13 074), in contrast to transgressive carbonatite (7 805 to 13 146 ppm, median of 9 681). Rare Earth Element distribution of phoscorite-hosted apatite shows a different degree of enrichment among the three phoscorite samples (Figure 5b).

Table 1. Results of U-Pb spot analysis of apatite from the Loolekop Pipe with B60Ph, B61Ph and GC813C phoscorite samples; GC813A and JKBC banded carbonatite samples; B63A and JKTC transgressive carbonatite samples.

Spot reference	$^{238}U/^{206}Pb$	±	$^{207}Pb/^{206}Pb$	±	Rho*	Spot reference	$^{238}U/^{206}Pb$	±	$^{207}Pb/^{206}Pb$	±	Rho*
B60Ph_1	2.375	0.058	0.175	0.003	0.904	GC813ABC_1	2.301	0.035	0.242	0.005	0.692
B60Ph_2	2.882	0.047	0.142	0.001	0.988	GC813ABC_2	2.282	0.030	0.211	0.003	0.601
B60Ph_3	2.725	0.260	0.151	0.005	0.840	GC813ABC_3	2.314	0.022	0.218	0.003	0.774
B60Ph_4	2.101	0.100	0.189	0.011	0.780	GC813ABC_4	2.509	0.051	0.197	0.005	0.774
B60Ph_5	2.574	0.050	0.159	0.002	0.796	GC813ABC_5	2.521	0.025	0.200	0.002	0.559
B60Ph_6	2.646	0.072	0.154	0.005	0.993	GC813ABC_6	2.492	0.043	0.214	0.005	0.820
B60Ph_7	2.594	0.041	0.165	0.002	0.669	GC813ABC_7	2.327	0.045	0.234	0.004	0.643
B60Ph_8	2.585	0.053	0.150	0.001	0.971	GC813ABC_8	2.257	0.087	0.225	0.012	0.956
B60Ph_9	2.533	0.048	0.156	0.003	0.958	GC813ABC_9	2.326	0.024	0.221	0.004	0.335
B60Ph_10	1.739	0.200	0.292	0.054	0.893	GC813ABC_10	2.409	0.053	0.213	0.003	0.572
B60Ph_11	2.577	0.070	0.148	0.003	0.909	GC813ABC_11	2.411	0.031	0.231	0.004	0.475
B60Ph_12	2.517	0.051	0.154	0.002	0.623	GC813ABC_12	2.372	0.039	0.216	0.003	0.731
B61Ph_1	2.822	0.068	0.180	0.002	0.883	GC813CPh_1	2.370	0.036	0.237	0.004	0.752
B61Ph_2	2.447	0.056	0.172	0.003	0.497	GC813CPh_2	2.354	0.033	0.254	0.004	0.611
B61Ph_3	2.352	0.042	0.198	0.003	0.599	GC813CPh_3	2.445	0.031	0.195	0.003	0.529
B61Ph_4	2.993	0.071	0.173	0.003	0.735	GC813CPh_4	2.459	0.039	0.161	0.002	0.304
B61Ph_5	2.384	0.045	0.196	0.003	0.668	GC813CPh_5	2.372	0.030	0.185	0.002	0.742
B61Ph_6	2.430	0.030	0.181	0.002	0.653	GC813CPh_6	2.387	0.120	0.186	0.006	0.897
B61Ph_7	2.472	0.040	0.158	0.002	0.486	GC813CPh_7	2.303	0.034	0.215	0.003	0.692
B61Ph_8	2.465	0.036	0.171	0.002	0.467	GC813CPh_8	2.262	0.056	0.195	0.005	0.669
B61Ph_9	2.439	0.030	0.171	0.003	-0.127	GC813CPh_9	2.384	0.038	0.157	0.002	0.670
B61Ph_10	2.370	0.033	0.185	0.003	-0.369	GC813CPh_10	1.969	0.045	0.272	0.004	0.723
B61Ph_11	2.500	0.022	0.168	0.002	-0.153	GC813CPh_11	2.254	0.048	0.193	0.004	0.631
B61Ph_12	2.431	0.032	0.177	0.002	0.448	GC813CPh_12	2.242	0.130	0.192	0.014	0.997
B61Ph_13	2.430	0.034	0.179	0.003	0.968	GC813CPh_13	2.141	0.045	0.208	0.009	0.457
B63A_1	2.123	0.330	0.172	0.007	0.925	JKCBC_1	3.509	0.290	0.195	0.003	0.989
B63A_2	0.431	0.120	0.717	0.062	0.885	JKCBC_2	2.145	0.039	0.196	0.002	0.894
B63A_3	2.474	0.045	0.189	0.009	0.574	JKCBC_3	2.202	0.046	0.197	0.006	0.831
B63A_4	2.518	0.042	0.173	0.003	0.481	JKCBC_4	2.151	0.030	0.227	0.006	0.585
B63A_5	2.541	0.038	0.167	0.002	0.741	JKCBC_5	2.030	0.037	0.281	0.003	0.931
B63A_6	2.439	0.057	0.195	0.003	0.947	JKCBC_6	2.137	0.034	0.235	0.003	0.766
B63A_7	2.551	0.074	0.208	0.007	0.604	JKCBC_7	2.208	0.062	0.231	0.006	0.807
B63A_8	2.793	0.320	0.176	0.009	0.850	JKTC_1	2.326	0.037	0.223	0.002	0.886
B63A_9	2.398	0.120	0.188	0.012	0.595	JKTC_2	1.063	0.062	0.588	0.014	0.938
B63A_10	2.425	0.055	0.183	0.003	0.809	JKTC_3	2.321	0.039	0.210	0.003	0.733
B63A_11	2.519	0.074	0.192	0.007	0.607	JKTC_4	2.320	0.033	0.216	0.002	0.728
B63A_12	1.992	0.110	0.310	0.030	0.938	JKTC_5	2.217	0.024	0.245	0.004	0.737
						JKTC_6	2.294	0.130	0.206	0.009	0.747

*Rho is an error correlation algorithm where rho=[(err $^{207}Pb/^{235}U$)2+(err $^{206}Pb/^{238}U$)2 - (err $^{207}Pb/^{206}Pb$)2]÷ [2×(err $^{207}Pb/^{235}U$)×(err $^{206}Pb/^{238}U$)].

Discussion
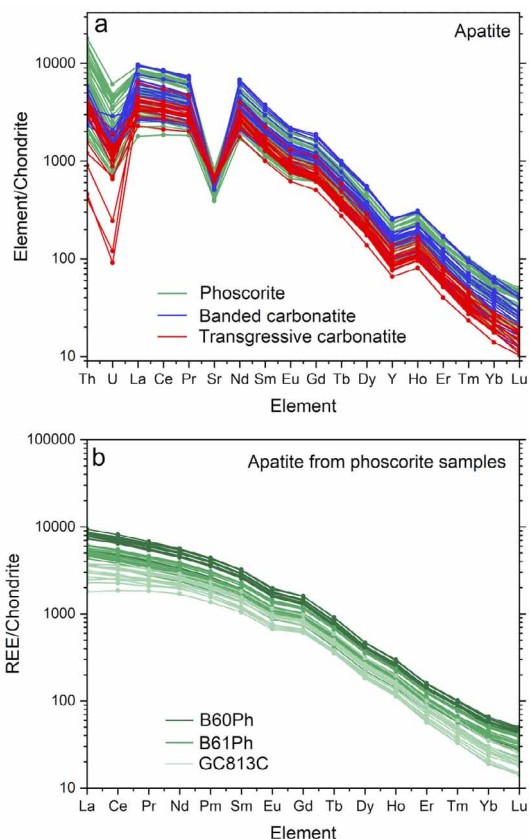### *An igneous origin for apatite*

Trace element concentrations and ratios in the studied apatite are typical of carbonatites globally (Belusova et al., 2002; Mao et al., 2016), and show LREE enrichment ((Ce/Yb)$_{ch}$ = 73-206), high V (3.44 to 24.1 ppm), Sr (2 828 to 5 991 ppm), and Ba (11.1 to 191 ppm) (Table 2 and Supplementary Material), in accordance with concentrations of these elements in carbonatitic melts (Bell, 1989; Hammouda et al., 2010; Jones et al., 2013). The Nb (0.02 to 0.58 ppm) and Zr (0.09 to 47.1 ppm) contents agree with averages in carbonatites (Chakhmouradian et al., 2017).

Rare Earth Elements, together with elements like U, Th, Y and Sr, can be used as geochemical tracers for discriminating between magmatic and hydrothermal apatite (e.g. Chen et al., 1993; Harlov, 2015; Chakhmouradian et al., 2017; O'Sullivan et al., 2020). Mafic magmatic apatite invariably shows consistent downward-sloping chondrite-normalised REE with relative LREE-enrichment and negative Eu anomalies, whereas a preferential LREE-depletion flattening the REE patterns, associated with a weaker negative, or even positive Eu anomaly, is indicative of hydrothermally-altered apatite (e.g. Broom-Fendley et al., 2016; Mao et al., 2016; Krneta et al., 2017; Zheng et al., 2022).

The geochemistry of the selected apatite from the Loolekop Pipe firmly attests to a magmatic origin (Figures 5a and 6). This is further supported by its high $(La/Yb)_{ch}$ ratio, in the range 70.7 to 238, while in hydrothermal varieties the ratio is commonly <25 (e.g. Chakhmouradian et al., 2017). Strontium is in the range 2 828 to 5 991 ppm, and values >2 000 ppm are considered diagnostic for magmatic apatite (Chakhmouradian et al., 2017). Thorium and U strongly partition into magmatic apatite, whereas the two elements are notably lower in hydrothermal apatite, as Th and U tend to form U-phases or concentrate in Fe-oxides (e.g. Krneta et al., 2017). In the studied apatite, Th reaches high tens to hundreds of ppm, and U is mostly >10 ppm, with Th/U relatively constant, ranging from 4.8 to 19.8.

Based on a reference database of apatite composition, Sr, Y and LREE contents can further refine the magma source and indicate an ultramafic igneous origin for these apatite (Figure 7, O'Sullivan et al., 2020)

Negative Eu/Eu* highlights competition between apatite, calcite and phlogopite during fractional crystallisation, in agreement with Decrée et al. (2020). No evidence for re-precipitation due to interaction with late-stage hydrothermal fluids, such as LREE depletion (O'Sullivan et al., 2020), can be observed in any apatite spot analysis. The slight inter-sample

Table 2. Chondrite-normalised REE ratio statistics for apatite from phoscorite, banded carbonatite and transgressive carbonatite. Chondrite composition from McDonough and Sun (1995). Data from Milani et al. (2017b).

Phoscorite	Median	Min.	Max.	10th percentile	90th percentile
$(La/Yb)_{ch}$	136	70.7	334	113	309
$(Ce/Yb)_{ch}$	123	73.2	238	103	225
$(La/Sm)_{ch}$	2.73	1.72	10.2	2.28	5.35
$(Sm/Lu)_{ch}$	65.0	23.6	92.5	56.2	84.2
Eu/Eu*	0.86	0.80	1.10	0.82	0.88
Sr/Y	17.9	14.2	24.3	14.6	22.1
ΣREE	12357	5908	51498	7931	47466
Banded carbonatite					
$(La/Yb)_{ch}$	160	114	213	122	204
$(Ce/Yb)_{ch}$	146	104	191	113	184
$(La/Sm)_{ch}$	2.48	1.34	2.88	2.03	2.76
$(Sm/Lu)_{ch}$	98.9	71.3	157	74.9	128
Eu/Eu*	0.86	0.67	0.90	0.78	0.89
Sr/Y	17.2	10.6	31.3	10.9	28.2
ΣREE	13074	8381	20897	9348	18105
Transgressive carbonatite					
$(La/Yb)_{ch}$	171	116	238	121	191
$(Ce/Yb)_{ch}$	157	111	206	115	177
$(La/Sm)_{ch}$	2.54	2.02	2.84	2.13	2.73
$(Sm/Lu)_{ch}$	100	77.4	124	80.4	118
Eu/Eu*	0.85	0.83	0.88	0.84	0.87
Sr/Y	33.3	23.1	43.9	24.0	38.8
ΣREE	9681	7805	13146	8662	10565

variation in REE, however, indicates that apatite in the Loolekop Pipe crystallised from a common, but variably enriched melt. Confirming the findings by Decrée et al. (2020), distinct REE patterns suggest repeated apatite crystallisation from progressively REE-depleted residual magmas (Figure 5b). Less common late-stage apatite at Phalaborwa, derived from rock interaction with hydrothermal fluids, follows an opposite trend, and tend to be progressively REE-enriched (Giebel et al., 2019). Transgressive carbonatite-hosted apatite shows a slightly different trace element signature with a higher Sr/Y ratio (Figure 7) and REE-depleted chondrite-normalised pattern relative to banded carbonatite (Figure 5a). This behaviour is difficult to explain, as O and Sr isotopes for phoscorite and carbonatite types suggest a common source with negligible crustal contamination (Decrée et al., 2020), which would prevent differences in REE distribution among the rocks at Loolekop. One possibility is to attribute the REE enrichment of banded carbonatite to new phases, like tetra-ferriphlogopite, added to the system and related to hydrothermal processes (Giebel et al., 2019). However, this does not seem to apply here, as no relevant post-magmatic alteration is apparent in apatite from banded carbonatite. Moreover, colour Cathodoluminescence (CL) imaging

Figure 5. (a) Chondrite-normalised multi element diagram showing compositions of apatite within the three rock types of the Loolekop intrusion. (b) Chondrite-normalised REE patterns for apatite from three phoscorite samples. Chondrite values from McDonough and Sun (1995).

of phoscorite and carbonatite in Decrée et al. (2020) revealed that late-formed apatite overgrowths along the crystal rims are systematically REE-depleted, thus suggesting that crystallisation from a more evolved melt at Phalaborwa produced a REE-depleted signature. The possible influence of variably evolved melts is particularly apparent in the phoscorite samples, which are variably REE-enriched (Figure 5b).

Apatite preservation

Patchy textures in BSE/CL images can be diagnostic of fluid-aided dissolution-reprecipitation (Odlum and Stockli, 2020), which may have been triggered by the circulation of late-stage magmatic fluids (Giebel et al., 2019). However, in this study, the patchy textures are not associated with differences in REE content, implying that the dissolution-reprecipitation process may have been different from the one described by Giebel et al. (2019). It is tempting to ascribe the dissolution-reprecipitation process to late-stage, valleriite-forming fluids (Le Bras, 2020), but direct evidence is lacking. Back Scattered Electron imaging of the Phalaborwa apatite reveals the occasional presence of patchy zoning and rare oscillatory zoning (Figure 3), which may point towards re-equilibration of apatite with the residual melt. However, the overall overlapping REE patterns in apatite from all rock types confirm that the grains did not undergo retrogressive recrystallisation or any relevant thermal perturbation. Some grains have BSE-dark rims which may indicate depletion in REE relative to cores (as in Figure 3a). We attribute this to crystal overgrowth due to a more differentiated magma pulse (e.g. Decrée et al., 2020).

A relatively rapid cooling

The U-Pb system in apatite represents a powerful tool to investigate the magmatic and thermal history of the crust (Chew and Spikings, 2015), and a detailed study to decipher the thermal history of the Kaapvaal Craton was recently presented by Baughman and Flowers (2018), who tested a multichronometer (U-Th)/He system on baddeleyite, zircon, titanite and apatite from Phalaborwa and the surrounding Archean basement of the Kaapvaal Craton. Their model, based on He diffusion in minerals, suggests that Phalaborwa cooled to surface temperatures by 1.4 Ga, likely followed by reheating events, required to explain a He resetting at 1.1 Ga, and with complete apatite resetting during the Karoo basin burial. However, their study did not clarify the extent to which the Phalaborwa Complex cooled just after its emplacement, as they generically assume cooling to <300°C by 2.0 Ga, based on a regional Rb-Sr study of muscovite and phlogopite in the northern Kaapvaal Craton (Barton and van Reenen, 1992).

The apparently undisturbed magmatic apatite ages obtained in this study are confirmed by the uniform distribution of trace elements in apatite from each sample. Together, these methods confirm relatively fast cooling of the carbonatite-phoscorite intrusion to at least ~350°C (closure temperature of the U-Pb system in apatite; Cochrane et al., 2014; Gawęda et al., 2014; Chew and Spikings, 2015, 2021), likely followed by a more protracted cooling at lower temperatures (Baughman and Flowers, 2018). According to the uncertainty resulting from the age determination, we can infer that the complex cooled below 350°C in no more than 21 Ma, meaning that cooling was a relatively fast process. This is in agreement with experimental
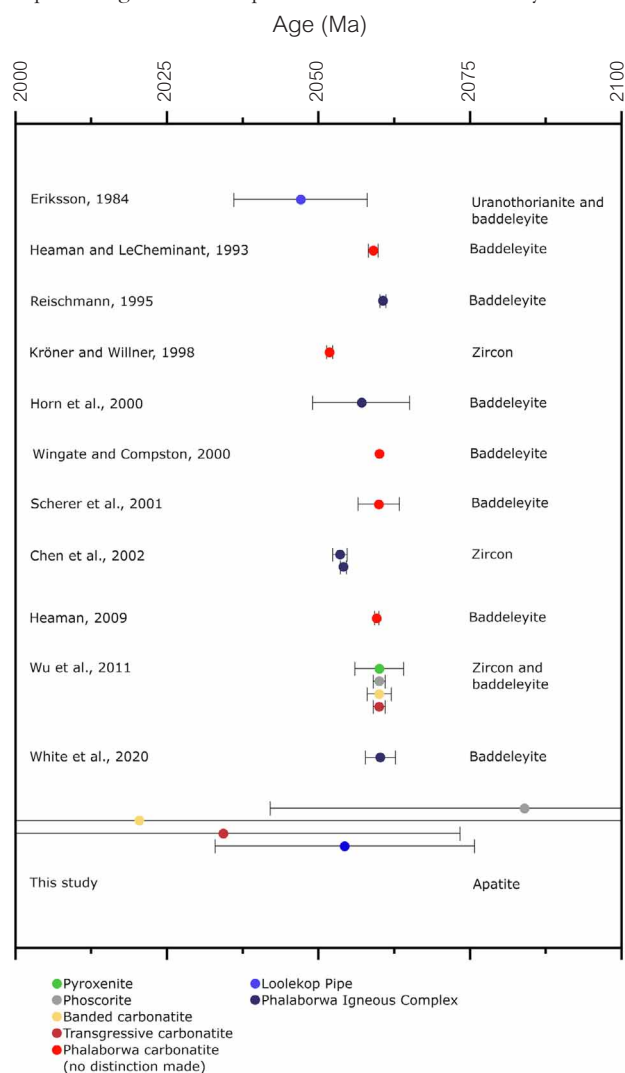
Figure 6. Summary of geochronological data for the Loolekop Pipe. Eriksson (1984): U-Pb analysis on uranothorianite and baddeleyite. Heaman and LeCheminant (1993), Reischmann (1995): U-Pb ages using TIMS. Kröner and Willner (1998): Pb-Pb dating with TIMS on zircon; Horn et al. (2000): baddeleyite U-Pb ages by LA-ICPMS analysis. Wingate and Compston (2000), Scherer et al. (2001): baddeleyite U-Pb TIMS. Chen et al. (2002), Heaman (2009): zircon and baddeleyite Pb-Pb TIMS. Wu et al. (2011), White et al. (2020): SIMS U-Pb and Pb-Pb. Reischmann (1995), Horn et al. (2000), Chen et al. (2002) and White (2020) do not mention a specific sample location, only the Phalaborwa Igneous Complex. Heaman and LeCheminant (1993), Kröner and Willner (1998), Wingate and Compston (2000), Scherer et al. (2001) and Heaman (2009) indicate a carbonatite origin for the analysed zircons and baddeleyites. Eriksson (1984) indicates a carbonatite and phoscorite origin for the analysed uranothorianites and baddeleyites. Wu et al. (2011), on the other hand, sampled zircons and baddeleyite in the three major rock types of the Loolekop Pipe.
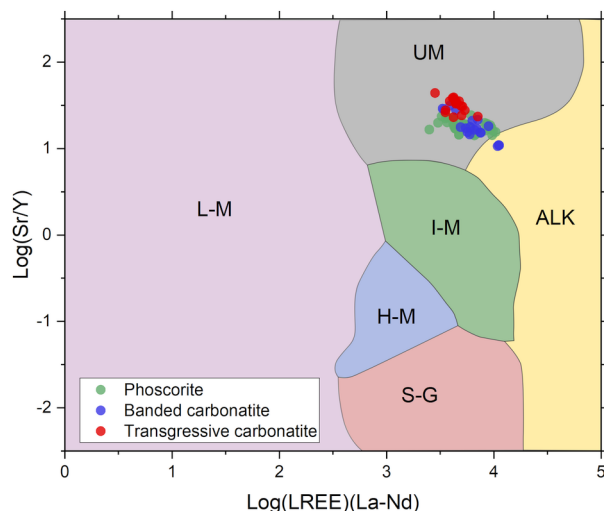
Figure 7. *Biplot of log(Sr/Y) versus log(LREE)(La-Nd) of apatite from rocks in Phalaborwa, compared to a discrimination scheme for apatite (O'Sullivan et al., 2020), based on machine learning using a large dataset of apatite from all common lithologies. Abbreviations: L-M=low- and medium-grade metamorphic and metasomatic apatite; H-M=high-grade metamorphic rocks; I-M=I-type granitoids and mafic igneous rocks; S-G=S-type granitoids; UM=ultramafic igneous rocks including carbonatites; ALK=alkaline igneous rocks (e.g. syenites).*

data on Ar diffusion kinetics in plagioclase from the coeval Bushveld Complex, which show that the complex cooled rapidly to temperature below 300°C in *ca.* 3 Ma (Cassata et al., 2009). Our data demonstrate the value of integrating mineral geochronometers sensitive to the medium-high part of the temperature history of a region (i.e. U-Pb and trace elements in apatite guided by CL/BSE imaging) to infer the higher-temperature part of the cooling history, and thus to infer emplacement dynamics of these rocks and complexes.

The apatite geochronometer applied to the Loolekop carbonatite-phoscorite intrusion

When apatite U-Pb data for all three principal rock types are combined, which is justifiable on the basis that all rocks yield identical ages within analytical uncertainty, an U-Pb date of 2 054.3 ± 21.4 Ma is obtained (Figure 4d). With an MSWD of 0.86, this age is consistent with derivation from a single intrusive event, or from pulses of magma very close in time. Therefore, we consider this age to reliably determine the emplacement timing of the Loolekop carbonatite-phoscorite complex. This age falls within the range of ages reported from U-Pb baddeleyite (2 060.0 ± 2.5 Ma, combined from Reischmann, 1995; Horn et al., 2000; Wingate and Compston, 2000; French et al., 2002; Heaman, 2009; Wu et al., 2011; White et al., 2020) and U-Pb zircon (2 053.5 ± 1.2 Ma, combined from Reischmann, 1995; Chen et al., 2002; Heaman, 2009; Wu et al., 2011) in the same rock types (Figure 6). The close agreement between all three mineral-isotope systems confirms that apatite can be used as geochronometer in the absence of other accessory minerals

(zircon and baddeleyite), to determine the age of magmatic systems, which were not affected by post-crystallisation thermal perturbation. However, as demonstrated by the age differences between phoscorite, banded and transgressive carbonatite, apatite U-Pb geochronology can show limitations in terms of precision in some mafic lithologies (*cf.* O'Sullivan et al., 2020). Apatite is less resistant to fluid-induced alteration and more sensitive to reheating than zircon and baddeleyite, making it a drawback in case of postdating reheating above 350°C as it resets the U-Pb system. Nevertheless, it can also be a significant advantage for the characterisation of emplacement processe(s) and timing of igneous intrusions and reheating when combined with higher temperature geochronometers.

Conclusions

In situ LA-SF-ICPMS analysis of U-Pb in apatite provides a combined age of 2 054.3 ± 21.4 Ma, MSWD = 0.86), which is identical within analytical uncertainty (though less precise), to ages obtained in previous studies by TIMS U-Pb analysis in both baddeleyite (2 060.0 ± 2.5 Ma) and zircon (2 053.5 ± 1.2 Ma). While our apatite U-Pb age is less precise than previous results, it permits inferences about cooling and emplacement history of the region unavailable from ultra-precise high-temperature geochronometers alone. In particular, the fact that apatite and other high-temperature geochronometers (zircon and baddeleyite) from the Loolekop Pipe all yield broadly similar ages means that the intrusion cooled below 350°C relatively soon after emplacement (<21 Ma). Furthermore, trace element compositions of igneous apatite from the Loolekop Pipe support a rapid emplacement of a progressively REE-depleted melt pulse from a common melt.

This study shows that *in situ* analysis of igneous apatite can be used to date phoscorite-carbonatite complexes, and that trace elements can aid interpretation of the U-Pb data by constraining the cooling rate, and ruling in or out later overprinting processes that may affect apatite, such as dissolution-reprecipitation during hydrothermalism. Combined U-Pb and trace elements in apatite can be advantageous considering the high abundance of apatite in these rock types. The less precise U-Pb age obtained from apatite compared to zircon and baddeleyite, is compensated by the ability to make additional inferences about the melt composition and cooling history of the intrusion post-emplacement. Furthermore, our results show that apatite is a viable detrital recorder of carbonatite and alkali magmatism, and the high modal abundance of apatite in these complexes raises the possibility of detecting apatite from carbonatite-phoscorite complexes in the detrital record when compared to other mineral geochronometers. Consequently, apatite may register the history of carbonatite magmatism in the detrital record, and thus help to elucidate processes of continental break-up or plume activity in long since eroded and denuded carbonatite complexes.

Acknowledgements

the samples. Professor Marlina Elburg, Dr. Sophie Decrée and an anonymous reviewer are thanked for their constructive comments that have helped to improve this paper. RB acknowledges financial support to establish the LA-SF-ICPMS facility at the University of Witwatersrand through a NRF-NEP grant (UID 105674). LM acknowledges support of the RDP (Research Development Program) at the University of Pretoria. The support of the DSI-NRF Center of Excellence for Integrated Mineral and Energy Resource Analysis (CIMERA) is acknowledged. Opinions expressed, and conclusions arrived at, are those of the authors and are not to be attributed to the DSI-NRF CIMERA.

Conflict of interests

The authors declare no conflict of interests.

References

Barton, J.M. and van Reenen, D.D., 1992. The significance of Rb-Sr ages of biotite and phlogopite for the thermal history of the central and southern marginal zones of the Limpopo Belt of Southern Africa and the adjacent portions of the Kaapvaal Craton. Precambrian Research, 55, 17-31.

Basson, I., Lourens, P., Paetzold, H.-D., Thomas, S., Brazier, R. and Molabe, P., 2017. Structural analysis and 3D modelling of major mineralizing structures at the Phalaborwa copper deposit. Ore Geology Reviews, 83, 30-42.

Baughman, J.S. and Flowers, R.M., 2018. Deciphering a 2 Gyr-Long Thermal History From a Multichronometer (U-Th)/He Study of the Phalaborwa Carbonatite, Kaapvaal Craton, South Africa. Geochemistry, Geophysics, Geosystems, 19, 1581-1594.

Bell, K., 1989. Carbonatites: Genesis and evolution, London, Unwin Hyman, 618pp.

Bolhar, R., Whitehouse, M.J., Milani, L., Magalhães, N., Golding, S.D., Bybee, G., Le Bras, L. and Bekker, A., 2020. Atmospheric S and lithospheric Pb in sulphides from the 2.06 Ga Phalaborwa phoscorite-carbonatite Complex, South Africa. Earth and Planetary Science Letters, 530, 115939.

Broom-Fendley, S., Styles, M.T., Appleton, J.D., Gunn, G. and Wall, F., 2016. Evidence for dissolution–reprecipitation of apatite and preferential LREE mobility in carbonatite derived late-stage hydrothermal processes. American Mineralogist, 101, 596-611.

Bulakh, A.G., Rudashevsky, N.S. and Karchevsky, P.I., 1998. Gold, silver, sulphides and rare-earth minerals in carbonatites of the Loolekop deposit (RSA). Zapiski Vserossiyskogo Mineralogicheskogo Obshchestva, 3, 45-54.

Cassata, W.S., Renne, P.R. and Shuster, D.L., 2009. Argon diffusion in plagioclase and implications for thermochronometry: A case study from the Bushveld Complex, South Africa. Geochimica et Cosmochimica Acta, 73, 6600-6612.

Chakhmouradian, A.R., Reguir, E.P., Zaitsev, A.N., Couëslan, C., Xu, C., Kynický, J., Mumin, A.H. and Yang, P., 2017. Apatite in carbonatitic rocks: Compositional variation, zoning, element partitioning and petrogenetic significance. Lithos, 274-275, 188-213.

Chen, F., Siebel, W. and Satir, M., 2002. Zircon U-Pb and Pb-isotope fractionation during stepwise HF acid leaching and geochronological implications. Chemical Geology, 191, 155-164.

Chen, W. and Simonetti, A., 2013. In situ determination of major and trace elements in calcite and apatite, and U-Pb ages of apatite from the Oka carbonatite complex: Insights into a complex crystallization history. Chemical Geology, 353, 151-172.

Chew, D.M., Sylvester, P.J. and Tubrett, M.N., 2011. U-Pb and Th-Pb dating of apatite by LA-ICPMS. Chemical Geology, 280, 200-216.

Chew, D.M. and Spikings, R.A., 2015. Geochronology and Thermochronology Using Apatite: Time and Temperature, Lower Crust to Surface. Elements, 11, 189-194.

Chew, D. M. and Spikings, R. A., 2021. Apatite U-Pb Thermochronology: A Review. Minerals, 11, 1095.

Chew, D.M., Sylvester, P.J. and Tubrett, M.N., 2011. U-Pb and Th-Pb dating of apatite by LA-ICPMS. Chemical Geology, 280, 200-216.

Cochrane, R., Spikings, R.A., Chew, D., Wotzlaw, J.-F., Chiaradia, M., Tyrrell, S., Schaltegger, U. and Van der Lelij, R., 2014. High temperature (>350°C) thermochronology and mechanisms of Pb loss in apatite. Geochimica et Cosmochimica Acta, 127, 39-56.

Dawson, J.B. and Hinton, R.W., 2003. Trace-element content and partitioning in calcite, dolomite and apatite in carbonatite, Phalaborwa, South Africa. Mineralogical Magazine, 67, 921-930.

Decrée, S., Cawthorn, G., Deloule, E., Mercadier, J., Frimmel, H. and Baele, J.-M., 2020. Unravelling the processes controlling apatite formation in the Phalaborwa Complex (South Africa) based on combined cathodoluminescence, LA-ICPMS and in situ O and Sr isotope analyses. Contributions to Mineralogy and Petrology, 175, 34.

Du Plessis, P.G., 2019. The parageneses of sulphide minerals in transgressive carbonatite of the Palabora Carbonatite Complex, South Africa. MSc. Thesis, University of the Free State, 194pp.

Eriksson, S.C., 1982. Aspects of the petrochemistry of the Phalaborwa Complex, Northeastern Transvaal, South Africa. PhD Thesis, University of the Witwatersrand, 495pp.

Eriksson, S.C., 1984. Age of carbonatite and phoscorite magmatism of the Phalaborwa Complex (South Africa). Isotope Geoscience, 2, 291-299.

Eriksson, S.C., 1989. Phalaborwa: a saga of magmatism, metasomatism and miscibility. In: K. Bell (Editor), Carbonatites: Genesis and evolution, vol. Unwin Hyman, London, 221-254pp.

French, J.E., Heaman, L.M. and Chacko, T., 2002. Feasibility of chemical U-Th-total Pb baddeleyite dating by electron microprobe. Chemical Geology, 188, 85-104.

Fourie, P.J. and de Jager, D.H., 1986. Phosphate in the Phalaborwa Complex. In: C.R. Anhaeusser and S. Maske (Editors), Mineral Deposits of Southern Africa, vol 2. Geological Society of South Africa, Pretoria, South Africa, 2239-2253.

Forster, I.F., 1958. Paragenetical Ore Mineralogy of the Loolekop-Phalaborwa Carbonatite Complex, Eastern Transvaal. South African Journal of Geology, 61, 359-365.

Gawęda, A., Szopa, K. and Chew, D., 2014. LA-ICP-MS U-Pb dating and REE patterns of apatite from the Tatra Mountains, Poland as a monitor of the regional tectonomagmatic activity. Geochronometria, 41, 306-314.

Giebel, R.J., Gauert, C.D.K., Marks, M.A.W., Costin, G. and Markl, G., 2017. Multi-Stage formation of REE Minerals in the Palabora Carbonatite complex, South Africa. American Mineralogist, 102, 1218-1233.

Giebel, R.J., Marks, M.A.W., Gauert, C.D.K. and Markl, G., 2019. A model for the formation of carbonatite-phoscorite assemblages based on the compositional variations of mica and apatite from the Palabora Carbonatite Complex, South Africa. Lithos, 324-325, 89-104.

Hammouda, T., Chantel, J. and Devidal, J.L., 2010. Apatite solubility in carbonatitic liquids and trace element partitioning between apatite and carbonatite at high pressure: Geochimica et Cosmochimica Acta, 74, 7220-7235.

Hanekom, H.J., Van Standen, C.M., Smit, P.J. and Pike, D.R., 1965. The Geology of Palabora Igneous Complex, South Africa. Geological Survey Handbook Memoir, 54, 185.

Harlov, D.E., 2015. Apatite: A Fingerprint for Metasomatic Processes. Elements, 11, 171-176.

Heaman, L.M., 2009. The application of U-Pb geochronology to mafic, ultramafic and alkaline rocks: An evaluation of three mineral standards. Chemical Geology, 261, 43-52.

Heaman, L.M. and LeCheminant, A.N., 1993. Paragenesis and U-Pb systematics of baddeleyite (ZrO₂). Chemical Geology, 110, 95-126.

Heinrich, E.W., 1970. The Palabora Carbonatitic Complex – A Unique Copper Deposit. Canadian Mineralogist, 10, 585-598.

Henrichs, I.A., O'Sullivan, G., Chew, D.M., Mark, C., Babechuk, M.G., McKenna, C. and Emo, R., 2018. The trace element and U-Pb systematics of metamorphic apatite. Chemical Geology, 483, 218-238.

Horn, I., Rudnick, R.L. and McDonough, W.F., 2000. Precise elemental and isotope ratio determination by simultaneous solution nebulization and laser ablation-ICP-MS: application to U-Pb geochronology. Chemical Geology, 164, 281-301.

Jones, A.P., Genge, M. and Carmody, L., 2013. Carbonate melts and carbonatites: Reviews in Mineralogy and Geochemistry, 75, 289-322.

Kirkland, C.L., Hollis, J., Danišík, M., Petersen, J., Evans, N.J. and McDonald, B.J., 2017. Apatite and titanite from the Karrat Group, Greenland; implications for charting the thermal evolution of crust from the U-Pb geochronology of common Pb bearing phases. Precambrian Research, 300, 107-120.

Kirkland, C.L., Yakymchuk, C., Szilas, K., Evans, N., Hollis, J., McDonald, B. and Gardiner, N.J., 2018. Apatite: a U-Pb thermochronometer or geochronometer? Lithos, 318-319, 143-157.

Krasnova, N.I., Petrov, T.G., Balaganskaya, E.G., Garcia, D., Moutte, J., Zaitsev, A.N. and Wall, F., 2004. Introduction to phoscorites: occurences, composition, nomenclature and petrogenesis. In: A. Zaitsev, F. Wall (Editors) Phoscorites and Carbonatites from Mantle to Mine: the key Example of the Kola Alkaline Province, vol 10. London, 43-72.

Krneta, S., Ciobanu, C.L., Cook, N.J., Ehrig, K. and Kontonikas-Charos, A., 2017. Rare earth element behaviour in apatite from the Olympic Dam Cu-U-Au-Ag Deposit, South Australia. Minerals, 7, 135.

Kröner, A. and Willner, A.P., 1998. Time of formation and peak of Variscan HP-HT metamorphism of quartz-feldspar rocks in the central Erzgebirge, Saxony, Germany. Contributions to Mineralogy and Petrology, 132, 1-20.

Le Bras, L. Y., 2020. Insights into sources and ore-forming processes of Cu-sulphide mineralization of the Phalaborwa Igneous Complex, from coupled Cu and Fe isotope and trace element systematics. PhD Thesis, University of the Witwatersrand, 234pp.

Le Bras, L.Y., Bolhar, R., Bam, L., Guy, B.M., Bybee, G.M. and Nex, P.A.M., 2021a. Three-dimensional textural investigation of sulfide mineralisation from the Loolekop carbonatite-phoscorite polyphase intrusion in the Phalaborwa Igneous Complex (South Africa), with implications for ore-forming processes. Mineralogical Magazine, 85, 514-531.

Le Bras, L.Y., Bolhar, R., Bybee, G.M., Nex, P.A.M., Guy, B.M., Moyana, T. and Lourens, P., 2021b. Platinum-group and trace elements in Cu-sulfides from the Loolekop pipe, Phalaborwa: implications for ore-forming processes. Mineralium Deposita, 56, 161-177.

Lombaard, A.F., Ward-Able, N.M. and Bruce, R.W., 1964. The Exploration and Main Geological Features of the Copper Deposit in Carbonatite Loolekop, Palabora Complex. In: S.H. Haughton (Editor), The geology of some ore deposits in Southern Africa, Geological Society of South Africa, Johannesburg, 315-337.

Mao, M., Rukhlov, A.S., Rowins, S.M., Spence, J. and Coogan, L.A., 2016. Apatite trace element compositions: A robust new tool for mineral exploration. Economic Geology, 111, 1187-1222.

McDonough, W. F. and Sun, S.-S., 1995. The composition of the Earth. Chemical Geology, 120, 223-253.

McDowell, F.W., McIntosh, W.C. and Farley, K.A., 2005. A precise ^{40}Ar-^{39}Ar reference age for the Durango apatite (U-Th)/He and fission-track dating standard. Chemical Geology, 214, 249-263.

Milani, L., Bolhar, R., Cawthorn, R.G. and Frei, D., 2017a. *In situ* LA-ICP-MS and EPMA trace element characterization of Fe-Ti oxides from the phoscorite-carbonatite association at Phalaborwa, South Africa. Mineralium Deposita, 52, 747-768.

Milani, L., Bolhar, R., Frei, D., Harlov, D.E. and Samuel, V.O., 2017b. Light rare earth element systematics as a tool for investigating the petrogenesis of phoscorite-carbonatite associations, as exemplified by the Phalaborwa Complex, South Africa. Mineralium Deposita, 52, 1105-1125.

O'Sullivan, G., Chew, D., Kenny, G., Henrichs, I. and Mulligan, D., 2020. The trace element composition of apatite and its application to detrital provenance studies. Earth-Science Reviews, 201, 103044.

O'Sullivan, G.J., Thakurdin, Y., Bolhar, R., Horváth, P., Hoare, B.C. and Collerson, K.D., 2021. The Great Falls Tectonic Zone after the assembly of Laurentia: evidence for long-term tectonic stability from xenolith apatite. Lithos, 384, 115977.

Odlum, M.L. and Stockli, D.F., 2020. Geochronologic constraints on deformation and metasomatism along an exhumed mylonitic shear zone using apatite U-Pb, geochemistry, and microtextural analysis. Earth and Planetary Science Letters, 538, 116177.

Paton, C., Hellstrom, J., Paul, B., Woodhead, J. and Hergt, J., 2011. Iolite: Freeware for the visualisation and processing of mass spectrometric data. Journal of Analytical Atomic Spectrometry, 26, 2508-2518.

Piccoli, P.M. and Candela, P.A., 2002. Apatite in Igneous Systems. Reviews in Mineralogy and Geochemistry, 48, 255-292.

Palabora Mining Company, 1976. The Geology and the Economic Deposits of Copper, Iron, and Vermiculite in the Palabora Igneous Complex: A Brief Review. Economic Geology, 71, 177-192.

Putnis, A., 2009. Mineral replacement reactions. Reviews in Mineralogy and Geochemistry 70, 87-124.

Reischmann, T., 1995. Precise U/Pb age determination with baddeleyite (ZrO$_2$), a case study from the Phalaborwa Igneous Complex, South Africa. South African Journal of Geology, 98, 1-4.

Scherer, E., Munker, C. and Mezger, K., 2001. Calibration of the lutetium-hafnium clock. Science, 293, 683-687.

Schoene, B. and Bowring, S.A., 2006. U-Pb systematics of the McClure Mountain syenite: thermochronological constraints on the age of the ^{40}Ar/^{39}Ar standard MMhb. Contributions to Mineralogy and Petrology, 151, 615-630.

Thomson, S.N., Gehrels, G.E., Ruiz, J. and Buchwaldt, R., 2012. Routine low-damage apatite U-Pb dating using laser ablation-multicollector-ICPMS. Geochemistry, Geophysics, Geosystems, 13, Q0AA21.

Vermeesch, P., 2018. IsoplotR: A free and open toolbox for geochronology. Geoscience Frontiers, 9, 1479-1493.

White, L.F., Tait, K.T., Kamo, S.L., Moser, D.E. and Darling, J.R., 2020. Highly accurate dating of micrometre-scale baddeleyite domains through combined focused ion beam extraction and U-Pb thermal ionization mass spectrometry (FIB-TIMS). Geochronology, 2, 177-186.

Wingate, M. and Compston, W., 2000. Crystal orientation effects during ion microprobe U-Pb analysis of baddeleyite. Chemical Geology, 168, 75-97.

Wu, F.-Y., Yang, Y.-H., Li, Q.-L., Mitchell, R.H. and Dawson, J.B., 2011. *In situ* determination of U-Pb ages and Sr-Nd-Hf isotopic constraints on the petrogenesis of the Phalaborwa carbonatite Complex, South Africa. Lithos, 127, 309-322.

Zheng, J., Shen, P. and Feng, W., 2022. Hydrothermal apatite record of ore-forming processes in the Hatu orogenic gold deposit, West Junggar, Northwest China. Contribution to Mineralogy and Petrology, 177, 27.

Editorial handling: M.A. Elburg.